Journal Pre-proof

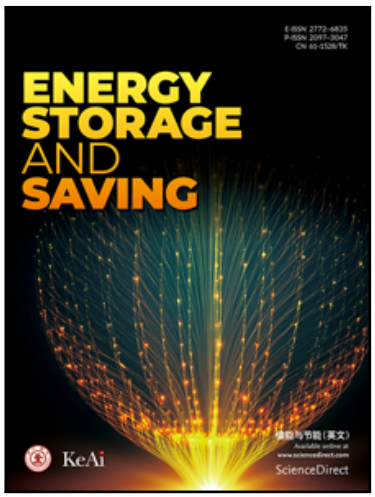

Thermodynamic modeling of non-equiatomic TiVNbCrAl-based lightweight refractory high-entropy alloys (LWRHEAs) for hydrogen storage applications

Ayotunde O. Aluko , Tien-Chien Jen , Sisa Pityana ,
Fredrick M. Mwema , Rasheedat Mahamood , Esther T. Akinlabi

PII: S2772-6835(26)00019-1
DOI: https://doi.org/10.1016/j.enss.2025.09.005
Reference: ENSS 148

To appear in: *Energy Storage and Saving*

Received date: 25 June 2025
Revised date: 15 August 2025
Accepted date: 12 September 2025

Please cite this article as: Ayotunde O. Aluko , Tien-Chien Jen , Sisa Pityana , Fredrick M. Mwema , Rasheedat Mahamood , Esther T. Akinlabi , Thermodynamic modeling of non-equiatomic TiVNbCrAl-based lightweight refractory high-entropy alloys (LWRHEAs) for hydrogen storage applications, *Energy Storage and Saving* (2026), doi: https://doi.org/10.1016/j.enss.2025.09.005

HIGHLIGHTS:

- **Alloys of non-equiatomic Ti-V-Nb-Cr-Al systems for hydrogen absorption storage were designed theoretically via HEAPS, CALPHAD, and PCT code.**
- **Both the VEC and δr parameters rises with the Nb/Cr/Al content, signifying rise in lattice distortion for increase in gravimetric capacity.**
- **Maximum hydrogen absorption capacity of the Nb-based alloy reaches 3.68wt.% with plateau pressure to ~1 bar at room temperature condition in the $Ti_{24}V_{24}Nb_{20}Cr_{16}Al_{16}$ alloy.**
- **A single-phase SS BCC structure was obtained predominantly for all the combination of different proportion of non-equiatomic TiVNbCrAl-based alloys.**

Thermodynamic modeling of non-equiatomic TiVNbCrAl-based lightweight refractory high-entropy alloys (LWRHEAs) for hydrogen storage applications

*Ayotunde O. Aluko[a,e], Tien-Chien Jen[a], Sisa Pityana[b], Fredrick M. Mwema[c], Rasheedat Mahamood[a,c], Esther T. Akinlabi[d]

[a]Department of Mechanical Engineering Science, University of Johannesburg, Johannesburg, 2029, South Africa;

[b]Photonics Center, Laser Enabled Manufacturing, CSIR, Pretoria, 0001, South Africa;

[c]Department of Mechanical & Construction Engineering, Faculty of Engineering & Built Environment, Northumbria University, Newcastle Upon Tyne, NE1 8ST, UK;

[d]Department of Mechanical Engineering, Colorado State University, Fort Collins, CO 80523, USA;

[e]Department of Mineral & Petroleum Resources Engineering, The Federal Polytechnic, Ado-Ekiti, 5351, Nigeria.

*Corresponding author: alayrehoboth@gmail.com; +27(0) 656301497

Abstract

Hydrogen, as a clean alternative energy carrier, is a key element in the global energy transition with great potential to significantly reduce the carbon footprint of transportation and other sectors. In this context, high-entropy alloys (HEAs) have emerged as promising candidates for hydrogen storage. Among them, refractory body-centered cubic (BCC)-based HEAs have demonstrated exceptional storage properties, achieving hydrogen-to-metal ratios up to 2.0 H/M, which motivates research into novel systems under moderate conditions. However, their practical application is hindered by thermodynamic and kinetic limitations, such as low-pressure conditions, difficult activation, high hydride stabilities, and consequently, high desorption temperatures. In this study, four lightweight refractory HEAs (LWRHEAs)—$Ti_{33}V_{33}Nb_{14}Cr_{10}Al_{10}$, $Ti_{30}V_{30}Nb_{16}Cr_{12}Al_{12}$, $Ti_{27}V_{27}Nb_{18}Cr_{14}Al_{14}$ and $Ti_{24}V_{24}Nb_{20}Cr_{16}Al_{16}$—were selected from eight candidates that satisfied empirical phase criteria and were predicted to form a single BCC solid solution; their hydrogen-storage properties were then systematically characterized. Pressure-composition-temperature (PCT) curves revealed an unusually high hydrogen uptake of ~2.0 H/M at 25 and 100 °C. The equilibrium plateau pressure increased steadily with composition, reaching nearly 1 bar for $Ti_{24}V_{24}Nb_{20}Cr_{16}Al_{16}$. Gravimetric capacity

indicated a steady, marginal variations with Nb/Cr/Al additions ranging from 3.60 to 3.68 wt% as the valence electron concentration (VEC) value increases, showing a remarkable capacity not commonly reported in BCC-based alloys. This study provides important insights into the compositional tuning of TiV-based BCC HEAs, demonstrating the effective synergy of Al/Cr additions with increased Nb content, and thereby offers guidance for the design of novel LWRHEAs for advanced hydrogen storage applications.

Keywords: CALPHAD-based method, Hydride, Hydrogen storage, TiVNbCrAl, Thermo-physical parametric calculations.

1 INTRODUCTION

Developing functional materials that place a premium on safety, efficiency, and economic storage is pivotal in driving the economic sustainability of hydrogen energy [1]. The development of alternative sources of energy to replace fossil fuels as the primary source of energy and carriers has become imperative to mitigate future global energy challenges owing to carbon emissions. It is on this premise that the Member States of the United Nations, regarding the global agenda a decade ago (2015), adopted the Sustainable Development Agenda for 2030. The Sustainable Development Goals (SDGs), in which SDG 7 is captured among the 17 goals, aim to ensure access to energy globally, affordably, reliably, and sustainably. Its motto is "Clean energy for all" [2]. Hydrogen is considered clean, affordable, renewable, and carbon-free compared to fossil fuels, and its products, which are mainly water vapor, are safe and harmless to the environment.

Research on environmentally carbon-free substitutes has been underway for several decades, and hydrogen energy has been regarded as a means to this end [3]. However, despite its great prospects, the high hydrogen density to gravimetric capacity in metallic materials is crucial to its potential for generation and storage [4,5].

However, the commercial demands for future hydrogen storage systems are still far-fetched according to the United States Department of Energy (DOE); and this ranges between 6.5 and 7.5 wt% for gravimetric density, while the storage conditions range from −40 to +150 °C in temperature and from 5 to 12 bar in pressure [6]. Compared to other options, solid-state metal hydride composition is the safest and most reliable storage mode that can meet such targets for mobile and stationary applications. High-entropy alloys (HEAs), among the various metal hydrides, are materials that can be tailored economically and technologically to meet these demands [7]. However, with several works that have been done to date on HEAs, the mechanism attributed to the properties of the hydrogen storage and their designs have remained unclear [8].

HEAs, also known as multi-principal element alloys, have received immense attention from both academia and industry for hydrogen storage-based metal hydrides because of the vast compositional fields that can be accessed. They are defined as alloys containing five or more principal elements, with each element's concentration ranging between 5 and 35 at.% [9,10]. The formation of HEAs is driven by the tendency to lower the Gibbs free energy through]an interaction between the enthalpy of mixing and the entropy of mixing. Specifically, the randomized simple phase solid solution formation is greatly enhanced compared to competing intermetallics when the entropy of mixing in metallic materials outweighs the enthalpy from the combination of multi-principal elements during solidification [11].

The main feature of HEAs is the formation of single- or multi-phase solid solutions. These phases derive their stability and high strength from fundamental material characteristics associated with 'core' effects of HEAs. As a result, they predominantly exhibit simple crystal structures such as body-centered cubic (BCC), face-centered cubic (FCC), or hexagonal close-packed (HCP), rather than intermetallic or other complex phases. These defining 'core' effects include high configurational entropy, lattice distortion (strain), sluggish diffusion, and the cocktail effect [12].

Various strategies have been attempted over the years to tune the hydrogen sorption performance, including the concept of binding-energy engineering, adjusting the atomic radii ratio, optimizing the chemical composition of the lightweight and transition elements, hydrogen affinity, and grain refinement [13,14]. Moreover, the storage properties of HEAs can be tuned by any strategy that raises the equilibrium plateau pressure above 1 bar. This increase lowers the onset desorption temperature, leading to effective hydride destabilization [15].

Theoretical design methods rely on thermophysical parameters such as valence electron concentration (VEC), electronegativity difference ($\Delta\chi^{A}$), enthalpy of mixing (ΔH_{mix}), entropy of mixing (ΔS_{mix}), atomic size mismatch (δ%), and atomic radius ratio (r_A/r_B), among others, to anticipate the formation of either simple- or multi-phase structured alloys. However, there are contradictory reports on which parameters drive the single-phase solid solution (SPSS) formation that offers prospects in a bid to design HEAs with larger A/B ratios by utilizing the benefits of BCC or laves structure [16,17]. Although thermodynamic empirical calculations are insufficient for the design of HEAs because of the intrinsic complexity of their composition, they have provided the means to quickly screen several alloys based on single- or multi-phase solid solutions and BCC structures. Many studies have reported that the BCC phase displays a better hydrogen-to-metal ratio, storage capacity, and hydrogen absorption/desorption kinetics than traditional alloys [18-20]. Several HEAs have been examined for hydrogen storage within the last decade [21], such as $Ti_5 + xV_{35}(CrMnFe)_{60-x\ (x = 0, 10, 20, 30)}$ [22], $Ti_{31}V_{26}Nb_{26}Zr_{12}M_5$ (M = Fe, Co or Ni) [23], ZrTiNiCrMn [24], $TiV_2ZrCrMnFeNi$ [25], TiZrNbMoV [26] and $Ti_{0.50-x}V_{0.25}Cr_xNb_{0.25\ (x = 0.15, 0.25, 0.30 \text{ and } 0.35)}$ [27] with the aim of optimizing their properties. However, further studies are imperative to construct these alloys by examining the thermodynamic properties and propensity of the chemical compositions to tune the hydrogen storage performance.

In light of the increasing quest for novel functional HEA-based materials that exhibit improved characteristics as stipulated by the US DOE, this study explored the use of empirical methods and thermodynamic modeling to simulate and predict the phase and metal hydride materials for reversible hydrogen storage applications. The non-equiatomic TiVNbCrAl-based lightweight refractory HEAs (LWRHEAs) compositions investigated in this work have not been reported in the literature.

The purpose of this research is to identify optimal stoichiometries of HEAs from the following lightweight and refractory transitional elements (Ti, V, Nb, Cr, Al) for developing room-temperature SPSS hydrogen storage systems using thermodynamic computational modeling tools. The specific objectives are: (1) to design SPSS-BCC HEAs samples using predictive tools (HEA predicting software (HEAPS), calculation of phase diagrams (CALPHAD), and pressure-composition-temperature (PCT) modeling); and (2) to model and simulate the most promising non-equiatomic TiVNbCrAl-HEA systems.

2 Materials and method

2.1 Selected materials in the LWRHEAs' design based on hydrogen storage

The performance integrity of an engineered material in use is predicated on the material behavior, which is directly dependent on the manufacturing process and the starting materials [28,29]. In this work, a strategy for BCC-HEA-based materials for hydrogen storage system design was proposed by utilizing the alloy's chemical composition and the combinatorial properties of a model 'TiV' binary system. The matrix was used to design LWRHEAs. The set of elements (Ti, V, Cr, Nb, Al) were carefully selected based on their unique characteristics and potential combinations, as suggested in the literature, and on the basis of the boundary conditions introduced in this study for maximum hydrogen storage performance. The primary rationale behind this selection is as follows:

(1) Nygård et al. [21] and Mayer Dias et al. [30] have shown that both Ti-V- and Ti-V-Cr-based HEAs systems are found to produce mainly the BCC phase structure, which is notable for its high hydrogen storage properties. Their studies have also shown that no activation treatment is required for equiatomic HEAs.

(2) Both Cr and Al are B-type, non-hydride formers with less negative enthalpies, and have been reported to yield less stable hydrides, resulting in higher plateau pressures suitable for hydride destabilization. Moreover, studies have also shown that increasing the Cr/Al content (>10 at.%) acts as a good hydride destabilizer, resulting in a lower hydrogen desorption temperature [31]. As a low-density element, Al enhances the stability of the BCC phase relative to other lightweight elements. This effect thereby lowers the onset temperature for hydrogen desorption and improves cycling properties [32]. The addition of Al also maintains a high H/M ratio, which concomitantly reduces the system's molar mass.

(3) High-melting-point refractory elements are known to enhance the thermodynamic stability of solid-solution HEAs. Among these, niobium (Nb), with its exceptionally high melting point 2,477 ℃ (2,750 K) and a BCC crystal structure at room temperature, plays a crucial role in stabilizing the BCC phase within the multicomponent solid solution. This stabilizing effect is attributed to the high-temperature processing conditions required for such alloys and the inherent structural compatibility [33,34]. Moreover, few Nb-based HEA compositions have been reported [35]. However, the ongoing examination seeks to explore the introduction of Nb for further groundwork in the field of Ti-V-Cr-based alloys to determine the mechanism attributed to its alloy hydriding/dehydriding.

2.2 Design conditions and basis for HEAs for hydrogen storage application

Some key concepts for the design of HEAs that can be deployed for hydrogen storage applications have been examined by Luo et al. [36] and Zhang et al. [37]. As verified in the literature, the conditions specified in designing SPSS-BCC-based HEAs for hydrogen storage systems should meet the minimum standards stipulated by the US DOE for onboard (mobile and stationary) applications. These include:

(1) The hydrogen gravimetric capacity should fall between 6.5 and 7.5 wt%, achievable within a temperature range of −40 to +150 ℃ and a pressure range of 5−12 bar. [6].

(2) HEAs systems must achieve hydride destabilization at an equilibrium plateau pressure above 1 bar to enable hydrogen release without compressors [30].

(3) HEAs should also exhibit excellent thermal cyclic stability (cyclability) and maintain their life-cycle performance over repeated hydrogen absorption/desorption cycles without degradation or pulverization [32].

2.3 Thermophysical parametric calculations

Just as the knowledge of Hume-Rothery rules has been used in the design of traditional alloys, the information gained from the thermophysical properties is crucial for anticipating the behavior of HEAs through modeling before the manufacturing process (Table 1) [38−45]. This is critical for determining the solubility of mixtures of elements in each other, and factors such as atomic size mismatch, crystal structure, valency, and electronegativity difference have been utilized. These factors influence the behavior of the mixture elements; for instance, whether the enthalpy of mixing (ΔH_{mix}) is negative, positive, or close to zero. Hence, LWRHEAs for room-temperature solid-state hydrogen storage are designed via a thermo-empirical-based method.

In the first step, the hydride formers A-type elements (Ti, V) and non-hydride formers B-type elements (Cr, Al) were combined in some non-equiatomic compositions. The element Nb is a weak hydride-forming element that was incorporated in increasing order to enhance the hydride stability of the LWRHEAs.

Second, boundary conditions were introduced to obtain configurations predominantly exhibiting a high tendency for BCC phase formation and to promote maximum hydrogen storage capacity. These key conditions and constraints are listed in Table 1.

The terms are defined as follows: $\Delta\chi^A$ is the Allen electronegativity difference, and C_i and C_j are the atomic percentages of the i-th and j-th components, respectively; r_i denotes the atomic radius; T_m represents the melting point calculated from the atomic percentage, and VEC_i is the valence electron concentration.

The various constraints introduced in this study are:

(1) Each element was prepared at a concentration of ≥10 at.% to ensure a high configurational entropy of mixing ($\Delta S_m \geq 1.5$ R) [46−48].

(2) The chromium (Cr) content was capped at 20 at.% to prevent the predominant formation of secondary phases (C14 Laves, HCP, FCC) over the desired BCC phase [49,50]. Beyond a threshold of ~10 at.%, Cr effectively increases the equilibrium plateau pressure, thereby reducing the thermodynamic stability of the hydride and lowering the desorption temperature. Additionally, interphase boundary formation in HEAs plays a crucial role in addressing the activation drawbacks and improving the absorption/desorption kinetics. Therefore, Cr must be carefully alloyed to serve a dual purpose: primarily to stabilize the BCC phase, and ultimately to optimize the hydrogen storage performance.

Table 1: Thermophysical parameters of the screened LWRHEAs, TiVNbCrAl for hydrogen storage properties

S/N	Parameter	Formulae	Condition of SPSS HEAs	Refs.
1	Electronegativity difference, ($\Delta\chi^A$)	$\Delta\chi^A = \sqrt{\sum_{i=1}^{n} C_i \left(X_i - \sum_{j=1}^{n} C_j X_j\right)2}$	$\Delta\chi^A > 7\%$ (Laves is present)	[38]

2	Mixing entropy, ΔS_{mix}	$\Delta S_{mix} = -R\sum_{i=1}^{n} X_i \ln X_i$	ΔS_{mix} > 12.47 J·mol^{-1}·K^{-1} where ΔS_{mix} = 1.5 R 11≤ΔS_{mix}≤19.5 J·mol^{-1}·K^{-1}	[39]
3.	Mixing enthalpy, ΔH_{mix}	$\Delta H_{mix} = \sum_{j\neq i}^{n}\sum_{i=1}^{n} 4\,\Delta H_{mixij} X_i X_j$	−22≤ΔH_{mix}≤7 kJ·mol^{-1}	[40]
4.	Atomic size mismatch, δ	$\delta = \sqrt{\sum_{i=1}^{n} C_i\left(1 - {r_i}/{\bar{r}}\right)2}$ $\bar{r} = \sum_{i=1}^{n} C_i\, r_i$	δ ≤ 6.6% δ > 5% (Laves is present)	[41]
5.	Intercepting parameter, Ω	$\Omega = \frac{T_m \Delta S_{mix}}{\Delta H_{mix}}$	Ω ≥ 1.1	[42]
6.	Atomic radii ratio, r_A/r_B	r_A/r_B	1.05−1.64 (Laves is present)	[43]
7.	Valence electron concentration, VEC	$VEC = \sum_{i=1} nC_i\,(VEC)_i$	VEC ≥ 8.0 for FCC VEC ≤ 6.87 for BCC VEC < 4.75 for HSC	[44]
8	Melting temperature	$T_m = \sum_{i=1}^{n} C_i\,(T_m)_i$		[45]

Note: HSC: hydrogen storage capacity; SPSS: single-phase solid solution; HEA: high-entropy alloy; LWRHEA: lightweight refractory HEA; FCC: face-centered cubic; BCC: body-centered cubic.

2.4 Alloy and hydride designing via thermodynamic calculation

The alloy compositions obtained by thermo-physical parametric calculations were carefully evaluated by Open CALPHAD CAE 0.1.0 version 2022 to check the phase stability based on the equilibrium conditions and the number of phases and confirm the possibility of BCC-phase formation.

An open-source code, written in Python, was employed to simulate PCT plots for the studied compositions. This was done to predict their hydrogen storage capacities (expressed as wt% or H/M) and the corresponding operating pressure and temperature conditions [51]. The fundamental principle of the code is based on the thermodynamic model by Zepon et al. [52], which uses the chemical composition of an alloy to design hydrogen storage systems. The simulated PCT plots were used to evaluate the hydrogen absorption capability of all eight LWRHEAs. Andrade et al. [8] studied

the interplay between the equilibrium plateau pressure (P_{equ}) and the hydrogen absorption/desorption temperature. $P_{equ.}$ is a key parameter for assessing the enthalpy and entropy changes required for hydride destabilization; therefore, a strategy is to maintain $P_{equ.}$ above 1 bar to achieve effective hydride destabilization [53,54].

3 Result and discussion

3.1 Thermodynamic properties of LWRHEAs, TiVNbCrAl by HEAPS

In Table 1, the thermodynamic empirical equations are the tools employed to optimize the parameters and calculate the properties (physical) of a set of HEAs, which satisfy the design conditions for hydrogen storage-based BCC-phase structures. The HEAPS code was employed to perform these calculations [42]. Table 2 lists the stoichiometries of the designed LWRHEAs, along with the results of the semi-empirical parameters to BCC phase formation and the tunability of hydrogen storage performance in the Ti-V-Nb-Cr-Al alloys. As shown in Table 2, the randomized solid-solution LWRHEAs were successfully designed, with all key parameters falling within the prescribed ranges for single-phase BCC-based HEAs (Table 1). Specifically, these key parameters include: (1) VEC, in which the values depict HEAs that fall, not only within the BCC phase, but also within the value for maximum hydrogen storage performance as stipulated by the US DOE, (2) the atomic size mismatch (δ) values obtained satisfying the condition reported in the literature, and (3) the electronegativity difference ($\Delta\chi^A$) values that satisfy the conditions for both BCC phase and Laves (C14) formations [50]. It is acknowledged that empirical parametric calculations have limitations for HEA design. Their predictive accuracy is constrained by the compositional complexity of HEAs, and they cannot determine the number of equilibrium phases or predict detailed phase diagrams [28]. However, they have provided a means to quickly screen several alloys as a preliminary approach to designing HEAs, which is complemented by the incorporation of a thermodynamic modeling method using the phase diagram technique (CALPHAD).

Table 2: Results of the semi-empirical parameters of the chemical composition of the optimized lightweight refractory high-entropy alloys (LWRHEAs)

Alloy composition (at.%)	Structure	VEC (-)	δ (%)	Ω (-)	ΔH_{mix} (kJ·mol^{-1})	ΔS_{mix} (J·mol^{-1}·K^{-1})	T_m (K)	$\Delta\chi^A$ (%)
$Ti_{33}V_{33}Nb_{14}Cr_{10}Al_{10}$	BCC	4.57	5.52	2.89	−8.69	12.20	2,057	9.7
$Ti_{30}V_{30}Nb_{16}Cr_{12}Al_{12}$	BCC	4.58	5.58	2.65	−9.79	12.68	2,051	10.0
$Ti_{27}V_{27}Nb_{18}Cr_{14}Al_{14}$	BCC	4.59	5.65	2.47	−10.8	13.02	2,044	10.2
$Ti_{24}V_{24}Nb_{20}Cr_{16}Al_{16}$	BCC	4.60	5.71	2.31	−11.71	13.25	2,038	10.4
$Ti_{21}V_{21}Nb_{22}Cr_{18}Al_{18}$	BCC	4.61	5.77	2.16	−12.53	13.35	2,031	10.6
$Ti_{18}V_{18}Nb_{24}Cr_{20}Al_{20}$	BCC	4.62	5.83	2.04	−13.25	13.33	2,025	10.7
$Ti_{15}V_{15}Nb_{26}Cr_{22}Al_{22}$	BCC	4.63	5.89	1.92	−13.88	13.18	2,018	10.8
$Ti_{12}V_{12}Nb_{28}Cr_{24}Al_{24}$	BCC	4.64	5.95	1.80	−14.82	12.89	2,012	10.8

Note: for max. hydrogen storage capacity VEC < 4.75 [44]. BCC: body-centered cubic; VEC: valence electron concentration.

3.2 Thermodynamic calculation of the designed LWRHEAs by CALPHAD technique

3.2.1 Equilibria phases

Fig. 1(a)−(g) show the equilibrium mole percent of the phases of the alloys studied and evaluated by an Open CALPHAD CAE 0.1.0 2022 version. The diagrams of the equilibrium phase mole percentage as a function of temperature calculated by CALPHAD indicate that all the alloys form, predominantly the BCC-phase structure (more than 60%) in the thermodynamic equilibrium condition. Moreover, the BCC-phase formed remained in the liquid phase and began to grow below 2,000 K until full solidification with a large interval. These intervals observed for all the studied LWRHEAs are higher than those reported by Mayer Dias et al. [30], where the proportion of hydride-formers (Ti, V) decreased with an increase in non-hydride formers (Cr, Al). However, the increase in weak hydride-forming elements (Nb) in the alloys may be attributed to this phenomenon, which results in increased solute partitioning (solidus temperature) upon solidification [33,34]. Studies have reported that elements with elevated melting points promote random formation of stable solid-solution structures at high processing temperatures. Hence, Nb, which has a high melting point, plays a crucial role in favoring and sustaining the BCC phase structure in the LWRHEAs solid solution [35]. These diagrams revealed regular trends in the amount of BCC phase formation, which may be attributed to many competing factors, including the incorporation of Al content, where studies confirmed it as a strong BCC phase (and its variants) stabilizer. However, the amount maintained at low temperatures (~800 K), particularly between Fig. 1(a)–(d), is significantly higher than that of some TiVCr- or TiVNbCr-based systems reported in the literature.

In addition to the high trend of BCC-phase formation, the thermodynamic equilibrium also revealed other phases at temperatures below 800 K with very low fractions (below 0.30) for alloys calculated under equilibrium conditions apart from Fig. 1(e)–(h). Notably, while the CALPHAD method predicts HCP and FCC as secondary phases at relatively low temperatures, the large range exhibited during the cooling process provides a high tendency for SPSS formation.

(a) (b)

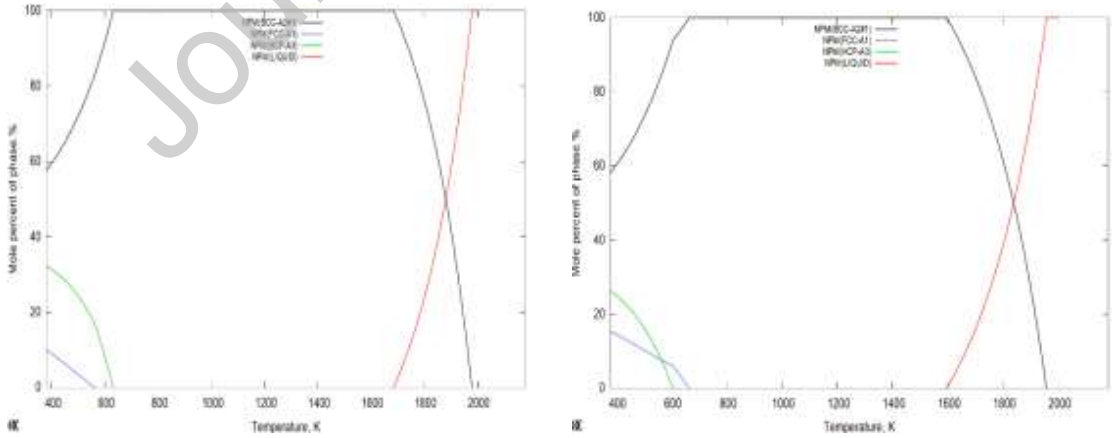

(c) (d)

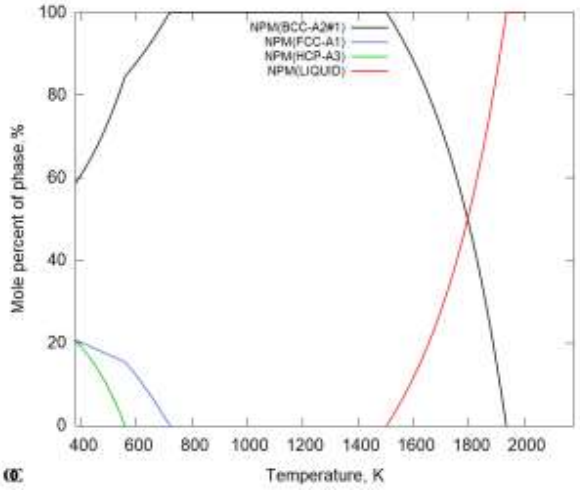

(e)

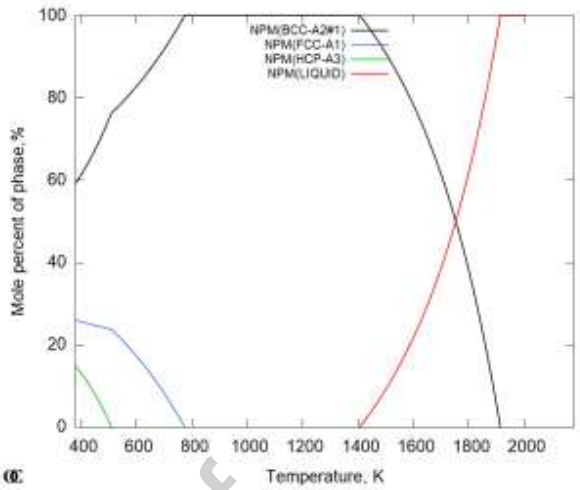

(f)

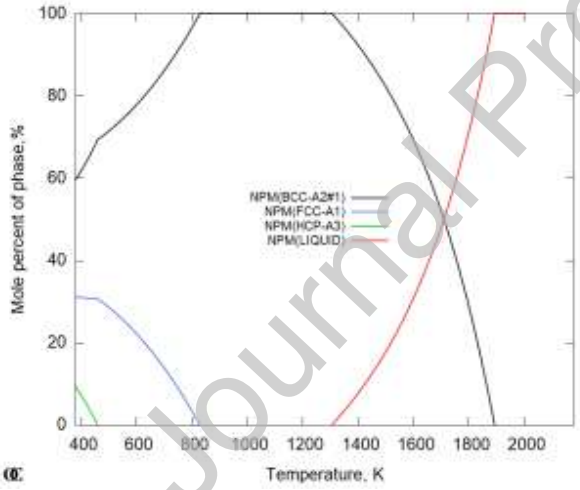

(g)

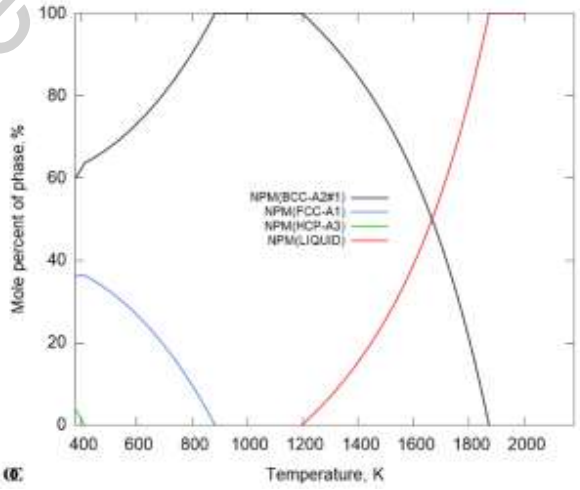

(h)

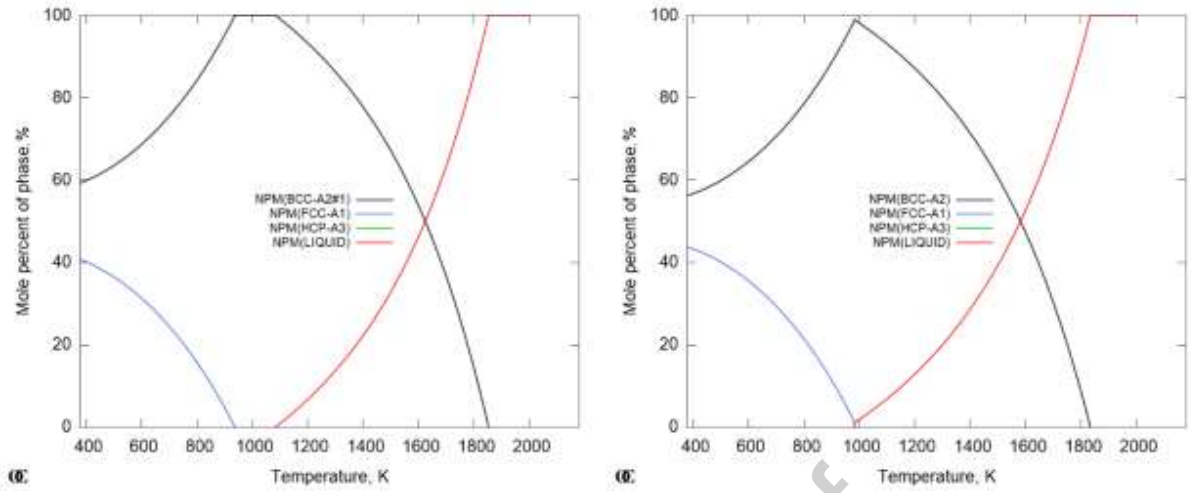

Fig. 1: CALPHAD-predicted equilibrium phase fractions (in mole percent) as a function of temperature for the eight lightweight refractory high-entropy alloys (LWRHEAs): (a) $Ti_{33}V_{33}Nb_{14}Cr_{10}Al_{10}$, (b) $Ti_{30}V_{30}Nb_{16}Cr_{12}Al_{12}$, (c) $Ti_{27}V_{27}Nb_{18}Cr_{14}Al_{14}$, (d) $Ti_{24}V_{24}Nb_{20}Cr_{16}Al_{16}$, (e) $Ti_{21}V_{21}Nb_{22}Cr_{18}Al_{18}$, (f) $Ti_{18}V_{18}Nb_{24}Cr_{20}Al_{20}$, (g) $Ti_{15}V_{15}Nb_{26}Cr_{22}Al_{22}$, (h) $Ti_{12}V_{12}Nb_{28}Cr_{24}Al_{24}$.

3.2.2 Simulation of PCT curves for the designed LWRHEAs

The PCT curve has become a tool for obtaining the parameters for the studied HEA compositions to predict the gravimetric capacity, as well as their corresponding operating conditions.

Fig. 2(a)–(d) present the PCT curves for four of the eight non-equiatomic TiVNbCrAl BCC-HEAs, calculated at both 25 and 100 °C. These alloys exhibit hydrogen storage capacities ranging from 3.60 to 3.68 wt% and approximately 2.0 H/M. The calculated alloys with the Cr/Al content beyond 16 atomic percent (at.%) recorded values below 3.5 wt% and did not produce any Van't Hoff plots while the absorption plateau pressures reveal values above 10^5 atm.

(a) (b)

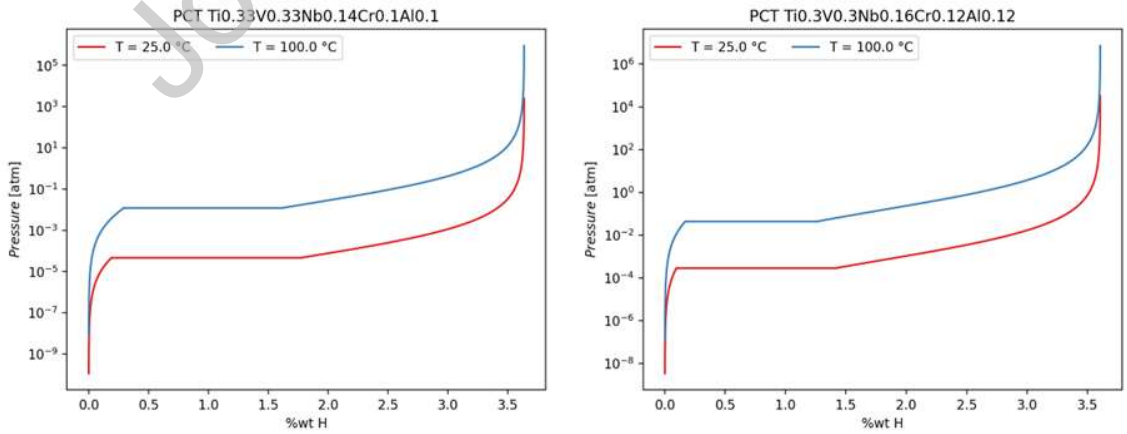

(c) (d)

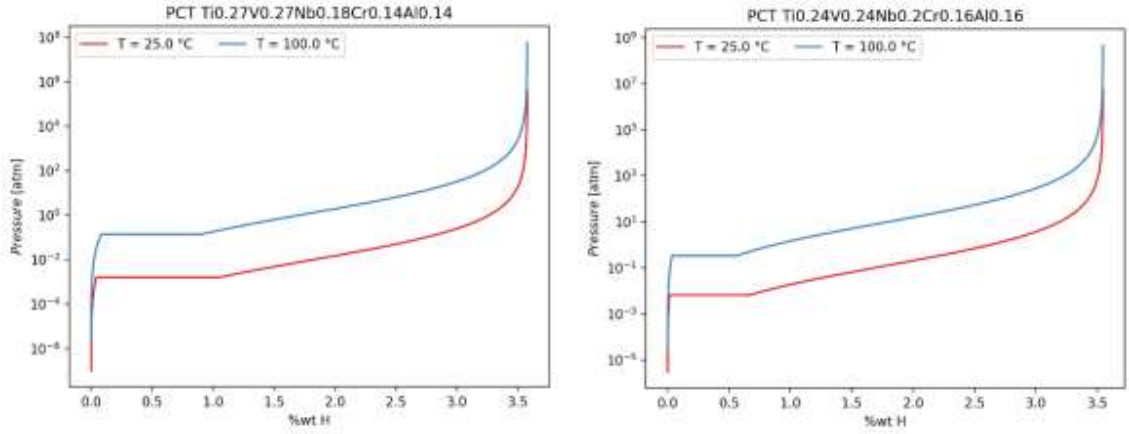

Fig. 2: Pressure-composition-temperature (PCT) curves at 25 and 100 ℃ for the four designed BCC-phase lightweight refractory high-entropy alloys (LWRHEAs): (a) $Ti_{33}V_{33}Nb_{14}Cr_{10}Al_{10}$, (b) $Ti_{30}V_{30}Nb_{16}Cr_{12}Al_{12}$, (c) $Ti_{27}V_{27}Nb_{18}Cr_{14}Al_{14}$, and (d) $Ti_{24}V_{24}Nb_{20}Cr_{16}Al_{16}$.

Nygård et al. [44] reported that HEA configurations with a VEC below 4.75 exhibit a high hydrogen capacity (>2.0 H/M). Furthermore, the formation of non-stoichiometric hydrides in HEAs, particularly those with higher VEC values (e.g., >5.00), can be influenced by the significant atomic size and electronegativity differences among the constituent elements.

Hence, all the LWRHEAs investigated exhibited VEC values within the range of 4.57–4.64, which is significantly below 4.75 (as shown in Table 2) within the design and boundary conditions introduced. Interestingly, this is confirmed from the PCT curves for all the studied LWRHEAs, yielding a high of 2.0 H/M (as the Cr/Al content increases). Moreover, studies have shown that careful substitution of hydride formers with non-hydride formers in TiVNb-based HEA materials enhances the absorption uptake (H/M) under moderate conditions. However, increasing the Cr/Al content beyond a critical value can reduce the gravimetric capacity (wt%) of TiVNbCr-based HEAs, which is similar to the findings of Pineda-Romero et al. [53] and Pineda-Romero and Zlotea [54]. Hence, a strategic balance is required in the composition to avoid maximum capacity loss.

There is a relationship between the non-hydride-forming elements and pressure ($P_{equ.}$), which is one of the factors that determines the hydrogen uptake performance of HEAs. In this study, the values of $P_{equ.}$ parameters increase as the Nb/Cr/Al content rises as against Ti/V ranging from 0.01 bar for $Ti_{33}V_{33}Nb_{14}Cr_{10}Al_{10}$ to ~1 bar for $Ti_{24}V_{24}Nb_{20}Cr_{16}Al_{16}$ alloy showing promising reversible hydrogen absorption properties.

4 Conclusions

This study investigated the prediction of the thermodynamic parameters, phase property characteristics, and hydrogen storage properties of non-equiatomic TiVNbCrAl BCC LWRHEAs for eight alloys. Four were selected in terms of their BCC phase/secondary composition to evaluate their potential for hydrogen storage. The results indicated that all the designed alloys satisfied semi-empirical conditions with the constraints introduced and exhibited a predominantly single-phase solid-solution BCC structure. Moreover, the increase in the Nb/Cr/Al content revealed a steady increase in $P_{equ.}$ pressure, reaching ~1 bar for the $Ti_{24}V_{24}Nb_{20}Cr_{16}Al_{16}$ alloy. Although all the alloys studied exhibited

significantly high 2.0 H/M at 25 and 100 ℃, the gravimetric capacity indicated a marginal variation (within the range of 3.60 to 3.68 wt%). Therefore, the incorporation of Cr/Al into hydrogen storage systems should be studied to determine the optimum properties and to further exploit their fine-tuning characteristics for hydrogen storage systems.

This work has demonstrated the significant effect of the combinatorial properties of Nb as a less negative enthalpy, weak hydride-forming element, and Cr/Al, as a promising strategy for further tuning of non-equiatomic TiVNbCrAl-based HEA configurations. The results reveal the potential for reversible hydrogen storage applications under moderate conditions, as shown by the CALPHAD-based method and PCT diagrams. However, the values of hydrogen storage properties are based on theoretical studies and hence require further experimental characterization and validation through hydrogenation testing.

Future work will focus on experimental procedures using a laser-engineered net shaping directed energy deposition additive manufacturing (LENS-DED AM) process for hydrogenation testing and different characterization methods.

Disclosure statement

The authors declare that they have no known competing financial interests or personal relationships that could have influenced the work reported in this study.

References

1. A.D. Akinwekomi, F. Akhtar, Bibliometric mapping of literature on high-entropy/multicomponent alloys and systematic review of emerging applications, Entropy 24 (2022) 329.

2. F.P. Martins, S. De-León Almaraz, A.B. Botelho Jr, et al., Hydrogen and the sustainable development goals: synergies and trade-offs, Renew. Sustain. Energy Rev. 204 (2024) 114796.

3. Y.F., Kao, S.K. Chen, J.H. Sheu, et al., Hydrogen storage properties of multi-principal component $CoFeMnTi_xV_yZr_z$ alloys, Int. J. Hydrog. Energy 35 (2010) 9046-9059.

4. B. Cheng, L. Kong, H. Cai, et al., Pushing the boundaries of solid-state hydrogen storage: a refined study on TiVNbCrMo high entropy alloys, Int. J. Hydrog. Energy 60 (2024) 282-292.

5. A. Mohammadi, Y. Ikeda, P. Edalati, et al., High-entropy hydrides for fast and reversible hydrogen storage at room temperature: binding-energy engineering via first-principles calculations and experiments, Acta Mater. 236 (2022) 118117.

6. Y.T. Zhai, Y.M. Li, S.H. Wei, et al., Progress in V-BCC based solid solution hydrogen storage alloys, J. Energy Storage 109 (2025) 115103.

7. S. Karpov, Application of high-entropy alloys in hydrogen storage technology, Probl. At. Sci. Technol. 2 (2024) 48-61.

8. G. Andrade, P. Edalati, S. Dangwal, et al., Microstructural characterization and hydrogen storage properties at room temperature $Ti_{21}Zr_{21}Fe_{41}Ni_{17}$ medium entropy alloy, ACS Appl. Energy Mater. 8 (2025) 2033-2042.

9. J.J. Zhang, J.T. Hu, H.Y. Xiao, et al., A first-principles study of hydrogen desorption from high entropy alloy TiZrVMoNb hydride surface, Metals 11 (2021) 553.

10. J.M. Torralba, M. Campos, High entropy alloys manufactured by additive manufacturing, Metals. 10 (2020) 639.

11. W. Zhang, A. Chabok, B.J. Kooi, et al., Additive manufactured high entropy alloys: a review of the microstructure and properties, Mater. Des. 220 (2022) 110875.

12. L.J. Kong, B. Cheng, D. Wan, et al., A review on BBC-structure high-entropy alloys for hydrogen storage, Front. Mater. 10 (2023) 1135864.

13. X.F. Ma, X. Ding, R. Chen, Enhanced hydrogen storage properties of $ZrTiVAl_{1-x}Fe_x$ HEAs by modifying the Fe content, RSC Adv. 12 (2022) 11272.

14. J. Liang, G.L. Li, X. Ding, et al., Formation of Zr-rich BCC phase and its relation on the hydrogen storage properties of TiVNbZr high entropy alloy, Int. J. Hydrog. Energy 48 (2023) 33610–33619.

15. R.B. Strozi, B.H. Silva, D.R. Leiva, et al., Tuning the hydrogen storage properties of Ti-V-Nb-Cr alloys by controlling the Cr/(TiVNb) ratio, J. Alloys Comp. 932 (2023) 167609.

16. J. Liang, G. Li, X. Ding, et al., Effect of C14 Laves/BCC on microstructure and hydrogen storage properties of $(Ti_{32.5}V_{27.5}Zr_{7.5}Nb_{32.5})_{1-x}$ Fe_x (x = 0.03, 0.06, 0.09) high-entropy hydrogen storage alloys. Journal of Energy Storage, 73 (2023) 108852.

17. P. Hájková, J. Horník, E. Čižmárová, et al., Metallic materials for hydrogen storage: a brief overview, Coatings 12 (2022) 1813.

18. R.R. Shahi, A.K. Gupta, P. Kumari, Perspectives of high entropy alloys as hydrogen storage materials, Int. J. Hydrog. Energy 48 (2023) 21412-21428.

19. S. Sleiman, J. Huot, Microstructure and first hydrogenation properties of $TiHfZrNb_{1-x}V_{1+x}$ alloy for x = 0, 0.1, 0.2, 0.4, 0.6 and 1, Molecules 27 (2022) 1054.

20. K. Nigutova, L. Oroszova, Z. Mokanova, D. Csik, K. Gaborova, J. Molliner, M. Lange, K. Saksl. Experimental validation of hydrogen affinity as a design criterion for alloys, Materials 17 (2024) 6106.

21. M. Usman. Hydrogen storage methods. Reviews and current status, Renew. Sustain. Energy Rev. 167 (2022) 112743.

22. Y.T. Zhai, Y.M. Li, L. Bolzoni, et al., Effect of heat treatment on microstructural evolution and hydrogen storage performance of as-milled $Ti_5+xV_{35}(CrMnFe)_{60-x}$ (x = 0, 10, 20, 30) high-entropy alloys, Int. J. Hydrog. Energy 81 (2024) 584-594.

23. L.F. Chancetti, B.H. Silva, J. Montero, et al., Structural characterization and hydrogen storage properties of the $Ti_{31}V_{26}Nb_{26}Zr_{12}M_5$ (M = Fe, Co or Ni) multiphase multicomponent alloys, Int. J. Hydrog. Energy 48 (2023) 2247-2255.

24. T. Fukagawa, Y. Saito, A. Matsuyama, Effects of varying Ni content on hydrogen absorption/desorption and electrochemical properties of Zr-Ti-Ni-Cr-Mn high entropy alloys. J. Alloys Comp. 896 (17) (2021) 163118.
25. S. Dangwal, K. Edalati, High-entropy alloy $TiV_2ZrCrMnFeNi$ for hydrogen storage at room temperature with full reversibility and good activation, Scr. Mater. 238 (2024) 115774.

26. I. Kunce, M. Polanski, I. Bystrzycki, Microstructure and hydrogen storage properties of a TiZrNbMoV high entropy alloy synthesized using laser engineered net shaping, Int. J. Hydrog. Energy 39 (2014) 9904-9910.

27. Z. Wen, G. Li, S. Wang, et al., Effect of C15 Laves phase ratios hydrogen absorption/desorption properties of $Ti_{0.50-x}V_{0.25}Cr_xNb_{0.25}$ (x = 0.15, 0.25, 0.30 and 0.35) multicomponent alloys, J. Alloys Comp. 1018 (2025) 179159.
28. U.S. Anamu, O.O. Ayodele, E. Olorundaisi, et al., Phase and mechanical property prediction of intermetallic-strengthening Ti-Al-Cr-Nb-Ni-Cu-Co high entropy alloys by thermo-physical parametric calculation and CALPHAD-based technique, MATEC Web Conf. 406, (2024) 06007.

29. J.W. Zhang, P.P. Zhou, Z.M. Cao, et al., Composition and temperature influence on hydrogenation performance of $TiZrHfMo_xNb_{2-x}$ high-entropy alloys, J. Mater. Chem. A 11 (2023) 20623.

30. G.C. Mayer Dias, B.H. Silva, A. de Sousa Martins, et al., Hydride destabilization in the Ti-Nb-Cr system through Nb/Ti ratio adjustment, ACS Appl. Energy Mater. 7 (2024) 6463-6474.

31. C. Kefi, J. Huot, Microstructure and first hydrogenation properties of $Ti_{30}V_{60}Mn_{(10-x)}Cr_x$ (x= 0,3.3, 6.6, 10) + 4 wt.% Zr, Metals 13 (2023) 1119.
32. Z. Ding, Y. Li, H. Jiang, et al., The integral role of high-entropy alloys in advancing solid-state hydrogen storage. Interdisciplinary Materials. 4(1) (2025) 75-108.
33. W. Chen, A. Hilhorst, G. Bokas, et al., A map of single-phase high-entropy alloys, Nat. Commun. 14 (2023) 2856.

34. F. Otto, Y. Yang, H. Bei, et al., Relative effects of enthalpy and entropy on the phase stability of equiatomic high-entropy alloys, Acta Mater. 61 (2013) 2628-2638.
35. J-Y. Yao, W. de Paula Santos, M. Moussa et al., Effect of Nb hydrogen storage properties of Ti-V-Cr-based alloys, Mater. Chem. Phys. 328 (2024) 130011.

36. L. Luo, L.P. Chen, L.R. Li, et al., High entropy alloys for solid hydrogen storage: a review, Int. J. Hydrog. Energy 50 (2024) 406-430.

37. Y. Zhang, Z.P. Lu, S.G. Ma, et al., Guidelines in predicting phase formation of high-entropy alloys. MRS Commun. 4 (2014) 57-62.

38. N. Yurchenko, N. Stepanov, G. Salishchev, Laves-phase formation criterion for high-entropy alloys, Mater. Sci. Technol. 33 (2017) 17–22.

39. M.G. Poletti, L. Battezzati, Electronic and thermodynamic criteria for the occurrence of high entropy alloys in metallic systems, Acta Mater. 75 (2014) 297-306.

40. Y. Zhang. X. Yang, P.K. Liaw, Alloy design and properties optimization of high entropy alloys, JOM. 64 (2012) 830-838.

41. J.W. Yeh, S.K. Chen, S.J. Lin, et al., Nanostructured high-entropy alloys with multiple principal elements: novel alloy design concepts and outcomes, Adv. Eng. Mater. 6 (2004) 299-303.

42. P. Martin, C.E. Madrid-Cortes, C. Cáceres, et al., HEAPS: a user friendly tool for the design and exploration of high-entropy alloys based on semi-empirical parameters, Comput. Phys. Commun. 278 (2022) 108398.

43. J.B. Ponsoni, V. Aranda, T. Nascimento, et al., Design of multicomponent alloys with C14 Laves phase structure for hydrogen storage assisted by computational thermodynamic, Acta Mater. 240 (2022) 118317.

44. M.M. Nygård, G. Ek, D. Karlsson, et al., Counting electrons - a new approach to tailor the hydrogen sorption properties of high-entropy alloys, Acta Mater. 175 (2019) 121-129.

45. X. Yang, Y. Zhang, Prediction of high-entropy stabilized solid-solution multi-component alloys, Mater. Chem. Phys. 132 (2012) 233-238.

46. M.M. Nygård, M.H., Sorby, A.A. Grimenes, et al., The influence of Fe on the structure and hydrogen sorption properties of Ti-V-based metal hydrides. Energies. 13 (2020) 2874.

47. K. Cardoso, V. Roche, A.M. Jorge, et al., Hydrogen storage in MgAlTiFeNi high entropy alloy. J. Alloys Comp. 858 (2021) 15837.

48. B.H. Silva, W.J. Botta, G. Zepon, Achieving room temperature hydrogen storage reversibility in Nb-rich alloys of the Nb-Cr-Mn system, J. Alloys Comp. 1005 (2024) 176187.

49. P.L.J. Conway, T.P.C. Klaver, J. Steggo, et al., High entropy alloys towards industrial application: high-throughput screening and experimental investigation, Mater. Sci. Eng. A 830 (2022) 142297.

50. J. Tau, C. Siyasiya, R. Modiba, et al., Investigation of hydrogen storage properties for high entropy alloys ($Ti_{30}V_{30}Cr_{30}Fe_{10}$ and $Ti_{40}V_{30}Cr_{10}Fe_{10}Al_{10}$), MATEC Web Conf. 406 (2024) 06008.

51. O.A. Pedroso, W.J. Botta, G. Zepon, An open-source code to calculate pressure-composition-temperature diagrams of multicomponent alloys for hydrogen storage, Int. J. Hydrog. Energy 47 (2022) 32582−32593.

52. G. Zepon, B.H. Silva, C. Zlotea, et al., Thermodynamic modelling of hydrogen-multicomponent alloy systems: calculating pressure-composition-temperature diagrams, Acta Mater. 215 (2021) 117070.

53. N. Pineda-Romero, M. Witman, V. Stavila, et al., The effect of 10 at.% Al addition on the hydrogen storage properties of the $Ti_{0.33}V_{0.33}Nb_{0.33}$ multi-principal element alloy, Intermetallics 146 (2022) 107590.

54. N. Pineda-Romero, C. Zlotea, Uncovering the effect of Al addition on the hydrogen storage properties of the ternary TiVNb alloy, Materials 15 (2022) 7974.

Declaration of interests

☒ The authors declare that they have no known competing financial interests or personal relationships that could have appeared to influence the work reported in this paper.

☐ The authors declare the following financial interests/personal relationships which may be considered as potential competing interests: